A99-27848 AIAA 99-1871

Computation of mixing layer noise using Large Eddy Simulation*

Christophe Bogey† Christophe Bailly‡and Daniel Juvé§

Laboratoire de Mécanique des Fluides et d'Acoustique
Ecole Centrale de Lyon & UMR CNRS 5509
BP 163, 69131 Ecully cedex, France.

Abstract

An LES code (ALESIA for Appropriate Large Eddy SImulation for Aeroacoustics) is developed using special techniques of Computational AeroAcoustics (CAA). This approach allows a direct determination of the compressible field by solving the filtered Navier-Stokes equations. A 2-D subsonic mixing layer between two flows at 40 and 160 $m.s^{-1}$ is simulated in a computational domain, including the acoustic far field. The sound generated by vortex pairing is then investigated. The radiation pattern has a characteristic double spiral structure with a wavelength given by the frequency of pairings. Generation noise mechanisms correspond to those proposed by Powell[1] and Mitchell[2] in their studies on two co-rotative vortices. The directly computed far-field sound is compared to the prediction of Lighthill's acoustic analogy[3] based on LES aerodynamic data. Results agree both with direct simulation and Colonius's works.[4]

1. Introduction

The aim of Computational AeroAcoustics (CAA) is to calculate acoustic fluctuations in flows, in order to provide reliable predictions to reduce noise radiation. CAA presents requirements[5,6] that have led to developments of specific techniques with respect to Computational Fluid Dynamics (CFD) methods. Indeed, the challenge is to compute acoustics very accurately in order to understand noise generation mechanisms.

Lighthill's analogy,[3] in 1952, was the starting point of modern aeroacoustics. It involves calculating the acoustic field via a volume integrale over the turbulent flow. Source terms are built up from aerodynamic data determined by solving Navier-Stokes equations or by generating a stochastic turbulent field.[7] This method requires the use of assumptions, i.e. the knowledge of Green's function and the neglection of convection and refraction effects. These assumptions limit the application of this method.

The direct calculation of an acoustic field is an alternative and more attractive method. Flow motion equations are solved to provide, simultaneously, aerodynamic and acoustic results, without restricting hypothesis and without modelling. Nevertheless, the direct approach has to face several difficulties linked to the great disparity between acoustic and aerodynamic fields. Acoustic perturbations are around 3 to 4 orders of magnitude smaller than aerodynamic perturbations, and this ratio is all the more significant when the flow is slow. Characteristic length scales are also very different, e.g. between the thickness of a mixing layer and the acoustic wavelength. Direct exploitation of the computed compressible field also requires accurate artificial boundary conditions, which have to minimize acoustic reflections at the domain limits.

Direct acoustic calculation is illustrated by simulations of Colonius,[4] Mitchell,[8] Mankbadi[9] and Freund.[10] Colonius has investigated a 2-D subsonic mixing layer by Direct Numerical Simulation (DNS). Mitchell and Mankbadi have studied axisymmetric jets with DNS and Large Eddy Simulation (LES) respectively. Freund has carried out a DNS of a full 3-D supersonic jet. In such supersonic flows, the dominant noise source is well identified. Supersonic convection of turbulent structures produces typically strong Mach wave radiation.

Noise generation mechanisms in subsonic flows are still being discussed. The goal of this work is to investigate the noise radiated by vortex pairing in a 2-D subsonic mixing layer. Colonius has demonstrated,[4] by filtering his DNS compressible field at

†Ph. D. Candidate

‡Assistant Professor, Member AIAA

§Professor, Member AIAA

the frequency of vortex pairing, that pairings generate acoustic radiation at that frequency. We propose to compute this noise directly by solving Navier-Stokes equations. A Large Eddy Simulation code (ALESIA for Appropriate Large Eddy SImulation for Aeroacoustics) is then developed with CAA techniques, in order to directly exploit the compressible field. Only larger scales are calculated, the smaller ones are modeled. Computation cost is then decreased compared to DNS, which is used to describe all turbulent structures. We also apply Lighthill 's analogy using Large Eddy Simulation. LES aerodynamic field is used to construct Lighthill's tensor.

In this paper, we present the simulation techniques, as well as the results of acoustic radiation in a mixing layer. The CAA techniques used to build the ALESIA code, and more importantly the numerical scheme and boundary conditions, are introduced in section 2. Flow characteristics and simulation specifications are described in section 3, and the compressible field computed directly by LES is shown in section 4. The noise mechanism associated to vortex pairing is described, and discussed in relation with other works.[1,2,4] Two integral formulations of Lighthill 's analogy are applied in section 5. Concluding remarks are given in section 6.

2. Numerical simulation algorithm

2.1 Governing equations

The full Navier-Stokes equations for two-dimensional fluid motion are written in the conservative form. In cartesian coordinates, we have

$$\frac{\partial U}{\partial t}+\frac{\partial Fe}{\partial x_1}+\frac{\partial Ge}{\partial x_2}-\frac{\partial Fv}{\partial x_1}-\frac{\partial Gv}{\partial x_2}=0 \qquad (1)$$

The variable vector U is given by

$$U=\begin{pmatrix}\rho\\ \rho u_1\\ \rho u_2\\ \rho e\end{pmatrix}$$

where ρ, u_1, u_2, ρe are the density, the axial and radial velocity components and total energy respectively. Fluxes are split into Euler fluxes, Fe and Ge, and the viscous fluxes, Fv and Gv.

The system (1) is completed by the definition of the total energy for a perfect gas, p being the pressure

$$\rho e=\frac{p}{\gamma-1}+\frac{1}{2}\rho(u_1^2+u_2^2)$$

where γ is the specific heat ratio. Thus, Euler fluxes are written as

$$Fe=\begin{pmatrix}\rho u_1\\ p+\rho u_1^2\\ \rho u_1u_2\\ (\rho e+p)u_1\end{pmatrix} \quad Ge=\begin{pmatrix}\rho u_2\\ \rho u_1u_2\\ p+\rho u_2^2\\ (\rho e+p)u_2\end{pmatrix}$$

and viscous fluxes as

$$Fv=\begin{pmatrix}0\\ \tau_{11}\\ \tau_{12}\\ u_1\tau_{11}+u_2\tau_{12}\end{pmatrix} \quad Gv=\begin{pmatrix}0\\ \tau_{21}\\ \tau_{22}\\ u_1\tau_{21}+u_2\tau_{22}\end{pmatrix}$$

The viscous stress tensor τ_{ij} is defined by

$$\tau_{ij}=2\mu S_{ij}$$

where μ is the dynamic viscosity and S_{ij} the deformation stress tensor given by

$$S_{ij}=\frac{1}{2}\left(\frac{\partial u_i}{\partial x_j}+\frac{\partial u_j}{\partial x_i}-\frac{2}{3}\delta_{ij}\frac{\partial u_k}{\partial x_k}\right)$$

2.2 Numerical scheme

Euler fluxes are primordial in acoustic phenomena because they supply the non-linear generation and propagation of sound. As a result, they need to be discretized by an accurate numerical scheme, the Dispersing Relation Preserving (DRP) scheme of Tam & Webb[11]:

$$\left(\frac{\partial Fe}{\partial x}\right)_{i,j}=\frac{1}{\Delta x}\sum_{l=-3}^{3}a_l Fe_{i+l,j}$$

This scheme has been developed to allow acoustic propagation over large distances. It has low dissipation and dispersion rates, and allows for acoustic waves with a minimum of 6 points per wavelength.

The spatial discretization is combined with a fourth-order Runge-Kutta method[12] for time integration. This algorithm requires low storage, and it is stable up to a CFL number CFL=$c_0(1+M)\Delta t/\Delta x$ equal to 1.73. (c_0 is the sound speed, M the Mach number, Δt and Δx time and space discretization steps)

The viscous fluxes are discretized with a centered second-order finite-difference scheme. These terms are then integrated in the last step of the Runge-Kutta algorithm. Indeed, these terms are less important for aeroacoustic mechanisms, because they do not operate directly on acoustic generation or propagation.

Finally, the equations are advanced in time in the following way

$$\begin{aligned}U_{i,j}^1 &= U_{i,j}^n+\alpha_1\Delta t Ke_{i,j}^n\\ U_{i,j}^2 &= U_{i,j}^n+\alpha_2\Delta t Ke_{i,j}^1\\ U_{i,j}^3 &= U_{i,j}^n+\alpha_3\Delta t Ke_{i,j}^2\\ U_{i,j}^{n+1} &= U_{i,j}^n+\alpha_4\Delta t Ke_{i,j}^3+\Delta t Kv_{i,j}^n\end{aligned}$$

where Ke et Kv are the integration terms of the Euler and viscous fluxes defined by

$$\begin{aligned} Ke^k_{i,j} &= -\sum_{l=-3}^{3} a_l \left(\frac{1}{\Delta x} Fe^k_{i+l,j} + \frac{1}{\Delta y} Ge^k_{i,j+l} \right) \\ Kv^n_{i,j} &= \frac{1}{2\Delta x} \left(Fv_{i+1,j} - Fv_{i-1,j} \right) \\ &+ \frac{1}{2\Delta y} \left(Gv_{i,j+1} - Gv_{i,j-1} \right) \end{aligned}$$

The selective damping of Tam[5] is used to filter numerical oscillations. These short waves are not supported by the numerical scheme, and are generated by boundary conditions or grid stretching. Damping terms are then added to the system (1), e.g. damping term in the axial direction is written as

$$\frac{\partial U}{\partial t} = ... - \frac{c_0}{R_s \Delta x} \sum_{k=-3}^{3} d_j \left(U_{i+k,j} - \bar{U}_{i+k,j} \right)$$

where R_s is the stencil Reynolds number, usually[5] $R_s = 5$ and $\bar{\mathrm{U}}$ is the mean flow value. These terms are integrated at the fourth step of the Runge Kutta, in the same way the viscous terms.

2.3 Boundary Conditions

Boundary condition formulation is a very important problem for acoustic computations. They have to minimize spurious waves produced when fluctuations leave the computational domain. Great care is then taken in order to exploit directly the acoustic field provided by Navier-Stokes calculations. Various formulations of boundary conditions and sponge zones have been tested before choosing the most accurate methods. Figure 1 describes the computational domain used in this study.

The nonreflecting boundary conditions of Tam & Dong[13] are implemented. They are more precise than the various approaches essentially based on characteristic equations. They are built from the asymptotic expressions of Euler's equations in the acoustic far-field. They are applied to three points, with DRP decentred schemes, and are integrated with the same Runge-Kutta method.

When only acoustic fluctuations reach the boundary, i.e. for inflow and lateral boundaries, the following radiation conditions are applied

$$\frac{1}{V_g} \frac{\partial}{\partial t} \begin{pmatrix} \rho \\ u_1 \\ u_2 \\ p \end{pmatrix} + \left(\frac{\partial}{\partial r} + \frac{1}{2r} \right) \begin{pmatrix} \rho - \overline{\rho} \\ u_1 - \overline{u}_1 \\ u_2 - \overline{u}_2 \\ p - \overline{p} \end{pmatrix} = 0$$

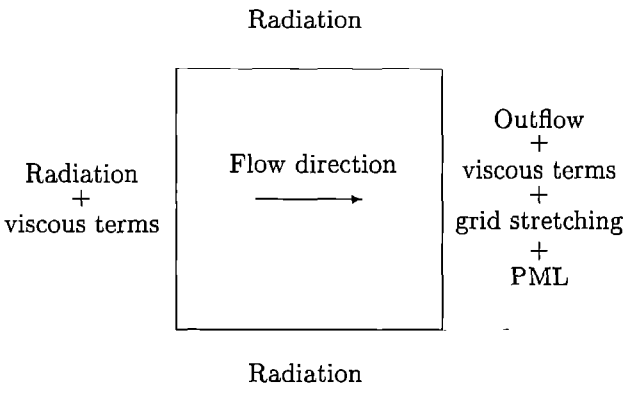

Figure 1: Boundary condition configuration for mixing layer simulations.

where $\overline{\rho}$, $\overline{u}_1$, $\overline{u}_2$, $\overline{p}$ are the mean density, velocity components and pressure respectively. V_g is the acoustic group velocity.[13]

Outflow boundary conditions are also necessary when aerodynamic fluctuations have to leave the domain, i.e. at the outflow boundary

$$\begin{cases} \dfrac{\partial \rho}{\partial t} + \overline{V}.\nabla \left(\rho - \overline{\rho} \right) = \dfrac{\partial p}{\partial t} + \overline{V}.\nabla \left(p - \overline{p} \right) \\ \dfrac{\partial u_1}{\partial t} + \overline{V}.\nabla \left(u_1 - \overline{u}_1 \right) = -\dfrac{1}{\overline{\rho}} \dfrac{\partial \left(p - \overline{p} \right)}{\partial x} \\ \dfrac{\partial u_2}{\partial t} + \overline{V}.\nabla \left(u_2 - \overline{u}_2 \right) = -\dfrac{1}{\overline{\rho}} \dfrac{\partial \left(p - \overline{p} \right)}{\partial y} \\ \dfrac{1}{V_g} \dfrac{\partial p}{\partial t} + \dfrac{\partial \left(p - \overline{p} \right)}{\partial r} + \dfrac{\left(p - \overline{p} \right)}{2r} = 0 \end{cases}$$

These boundary conditions were successfully validated with the ICASE test cases,[14] i.e acoustic pulse and vortex. The exit of vortical structures generates weak spurious acoustic waves, typically a few per cent of the incoming perturbations. Unfortunately, these small parasite waves are not negligible with respect to the acoustic field.

A sponge zone is then built to dissipate aerodynamic fluctuations before their reaching the outflow boundary. Two methods are combined. Firstly, the mesh is stretched in the axial direction in order that the turbulent structures are not supported by the numerical scheme. Secondly, a damping term is added in the equations to avoid reflection produced in the sponge zone layer travelling in the upstream direction. The technique called Perfectly Matched Layer (PML) proposed by Berenger[15] is used, with

the following additional term in the system (1)

$$\frac{\partial U}{\partial t} = \ldots - \frac{c_0 \sigma(x,y)}{\Delta x}\left(U - \bar{U}\right)$$

with for exemple

$$\sigma(x,y) = \sigma_{max}(x,y)\left(\frac{x - x_o}{x_{max} - x_o}\right)^2$$

where $\sigma_{max} = 0.15$, x_o and x_{max} are the locations at the beginning and the end of the PML zone.

Viscous fluxes are also integrated in inflow and outflow boundaries, to avoid discontinuity in the viscous terms.

2.4 Subgrid Scale Model

In Direct Numerical Simulation, all turbulent scales have to be calculated. This is often difficult with the computer ressources available, and so restricts DNS applications to low Reynolds number flows.

When DNS is proscribed, Large Eddy Simulation is an alternative for computing less canonical flows. It consists of calculating larger structures. However, effects of smaller scales are taken into account via a subgrid scale model. Turbulent viscosity ensures dissipation of the smaller unresolved structures, and allows us to write the subgrid scale stress tensor as

$$\tilde{\tau}_{ij} = 2\mu_t S_{ij}$$

Various models have been built to determine this turbulent viscosity. To keep the problem as simple as possible for aerodynamics, we choose Smagorinsky's model[16]

$$\mu_t = \rho\left(C_s \Delta_c\right)^2 \sqrt{2 S_{ij} S_{ij}}$$

where the Smagorinsky constant is taken to be $C_s = 0.18$, and the characteristic grid length is $\Delta_c = \sqrt{\Delta x \Delta y}$.

A more sophisticated subgrid scale model could be used.[17] In this study, our efforts are directed towards the exploitation of the compressible field, and more particularly the boundary conditions. In a further study, it would be interesting to discuss the impact of the subgrid scale model on aeroacoustics.

3. Flow simulation

3.1 Flow parameters

A 2-D mixing layer is defined by the following inflow hyperbolic tangent velocity profile, as represented in figure 2

$$u_1(y) = \frac{U_1 + U_2}{2} + \frac{U_2 - U_1}{2}\tanh\left(\frac{2y}{\delta_\omega(0)}\right)$$

where U_1 and U_2 are velocities of the slow and rapid flows respectively, and $\delta_\omega(0)$ the initial vorticity thickness. One also defines the convection velocity as $U_c = (U_1 + U_2)/2$ =100 m.s^{-1}.

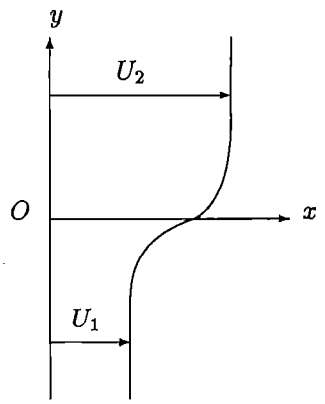

Figure 2: Mixing layer configuration.

The two flows are U_1=40 m.s^{-1} and U_2=160 m.s^{-1}. The velocity difference is moderate between the two flows, since the relative convection Mach number is $M_c = (U_2 - U_1)/2 = 0.176$.

The Reynolds number of the mixing layer based on the vorticity thickness is equal to $Re_\omega = \delta_\omega(0)(U_2 - U_1)/\nu = 12800$. This medium Reynolds number limits the subgrid scale model viscosity to a reasonable value, typically of the order of molecular viscosity.

3.2 Numerical specifications

The computational mesh has 441 × 441 points. Minimum mesh spacing in the axial and radial directions are $\Delta x = 0.32\ \delta_\omega(0)$ and $\Delta y = 0.16\ \delta_\omega(0)$. Points are concentrated in the shear zone, and mesh stretching is 1.8 % on each side of the radial direction. Mesh spacing is constant in the axial direction up to the last 100 points where a 2.8 % stretching is applied to form the sponge layer.

PML term is added with a parabolic profile from $X = 130\ \delta_\omega(0)$ to the outflow boundary. A radial weighting of this term is also applied to make it zero outside the mixing layer. In this way, the sponge zone dissipates vortices in the mixing layer but not the acoustic radiation outside, because the acoustic wavelength is high enough to still be supported by the stretched mesh.

Finally, the physical portion of the computational domain extends to 200 $\delta_\omega(0)$ in the axial direction, and from -300 $\delta_\omega(0)$ up to 300 $\delta_\omega(0)$ in the radial direction.

The time step is defined by $\Delta t = \Delta y_{min}/c_0$. The simulation runs for 10^4 iterations and is 1 hour long on a C-98 Cray (1.6×10^{-6} seconds per point and per iteration, and a CPU speed of 500 Mflops).

3.3 Inflow forcing

Several experiences have demonstrated the importance of large coherent structures in turbulence,[18-20] and it is particulary true for low Reynolds number flows. Crow & Champagne[18] have also shown that large structures can exhibit organized behaviour when subjected to a suitable excitation.

In order to govern the development of the mixing layer, an excitation is introduced into the inflow. The flow is forced at the inflexion point of the profile by adding vortical perturbations to velocity at every iteration. An harmonic excitation with pulsation ω is defined as

$$\begin{cases} u_1(x,y,t) = u_1(x,y,t) + \dfrac{(y-y_0)}{\Delta y_0} E \sin(\omega t) \\ u_2(x,y,t) = u_2(x,y,t) - \dfrac{(x-x_0)}{\Delta y_0} E \sin(\omega t) \end{cases}$$

where E is the gaussian weighting defined by

$$E = \alpha U_c \exp\left(-\ln(2)\frac{(x-x_0)^2 + (y-y_0)^2}{\Delta y_0^2}\right)$$

x_0 and y_0 are the location of the excitation. The coefficient α is around 10^{-3}, which is weak enough not to produce significant spurious waves.

3.4 Aerodynamic Results

Actually, the mixing layer flow is forced at two frequencies: its fundamental frequency f_0 and its first subharmonic $f_0/2$. The fundamental frequency corresponds to the most amplified instabilities, predicted by the linear theory of Michalke,[21] and is written as

$$f_0 = 0.136 \frac{U_c}{\delta_\omega(0)}$$

This excitation allows control of the vortex pairing: their locations are fixed around $X = 70\ \delta_\omega(0)$ as shown on figure 3; and vortex pairings occur at a frequency equal to $f_0/2$.

The numerical solution is in agreement with experimental visualizations of Winant & Browand.[20] Their study has described the vorticity field associated to vortex pairing in mixing layer.

The sponge zone is effective from $X = 150\ \delta_\omega(0)$, and dissipates vortices before other pairings happen downstream.

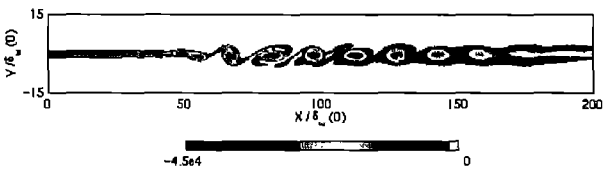

Figure 3: Vorticity field computed by exciting the mixing layer at the two frequencies f_0 and $f_0/2$, levels given in s^{-1}.

A broadband excitation has also been applied to simulate natural development of the mixing layer. The linear spatial growth, turbulence rates and spectra are not shown in this paper, but they conform to previous similar studies.[19,22]

4. Direct calculation of the acoustic field

Vortex pairing consists of the process of two structures rotating around each other before sudden merger. Previous works[20] have suggested that this typical non-linear phenomenon constitutes a major acoustic source in subsonic flows. However it has been refuted for general flows.[23] Nevertheless, in low-Reynolds number flows, fine scale turbulence is negligible and vortex pairing can be regarded as the dominant noise source in the mixing layer.

The first simulation of noise radiated by a mixing layer ($U_1 = c_0/4, U_2 = c_0/2, Re_\omega = 250$) was carried out by Colonius.[4] He has shown that vortex pairing generates a downstream acoustic radiation, with a wavelength in accordance with the frequency of pairings $f_p = f_0/2$. So we can expect in our simulation to find an acoustic frequency of f_p, corresponding to an acoustic wavelength equal to $\lambda_{f_p} = 51.5\ \delta_\omega(0)$ in a medium at rest.

Figure 4 displays the dilatation field $\Theta = \nabla.\mathbf{u}$ calculated by ALESIA on the whole computational domain. Wave fronts are observed coming from the location of the pairings. The acoustic wavelength is comparable to λ_{f_p}, as expected. However, wavelengths are modulated by convection effects induced by the two flows. Moreover, wave fronts are ovalized, which is especially visible for the upper flow, corresponding to the rapid velocity.

Acoustic radiation is well marked in the downstream direction, and even more precisely for angles close to $\theta_1 = 80°$ for the lower flow and $\theta_2 = 60°$ for the upper flow. The difference between θ_1 and θ_2 can also be attributed to convection effects. Results are in fair agreement with Colonius's works, if we

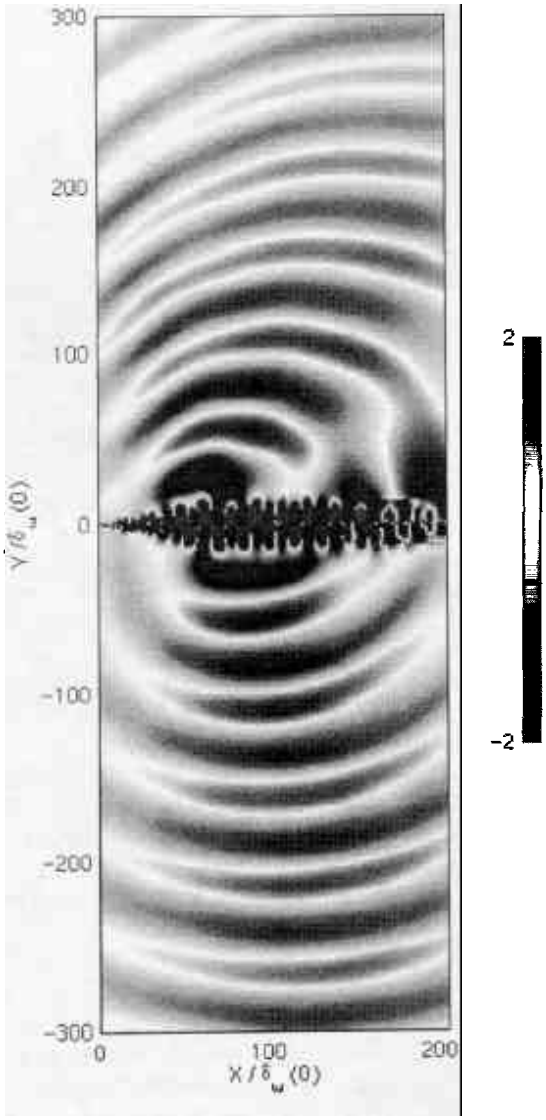

Figure 4: Dilatation field $\Theta = \nabla.\mathbf{u}$ computed on the whole calculation domain, levels given in s^{-1}.

note that the two velocites of his mixing layer are higher.

Levels of the dilatation field are around 2 s^{-1}, corresponding to 10 Pa for the pressure field. This value is small compared to the aerodynamic pressure fluctuations, which are greater than 1000 Pa. This result validates all the work on the boundary conditions, since no spurious waves are left undetected in the compressible field.

Figure 5 displays four views of the pairing zone. The vorticity field is superimposed on the dilatation field on the shear layer. The views are regularly spaced over a period $T_p = 1/f_p$, defined as the time between two subsequent vortex pairings. The time step between two pictures is $T_p/4$, a period pairing is described by figures (a)-(b)-(c)-(d)-(a) respectively. These pictures allow us to propose the noise mechanism associated to vortex pairing.

A double spiral structure is observed, in particular in figure 5-(b). The analytical works of Powell,[1] and numerical simulations of Mitchell[2] dealing with the noise generated by two co-rotative vortices present a similar radiation pattern. Powell has identified this source as a rotating quadrupole with four typical lobes.

We can detail the different steps of a pairing. In Figure (a), two neighboring vortices begin to roll around each other: this is the starting point of acoustic radiation. In Figure (b), a second radiation lobe appears perpendicular to the first one, which is now represented as a single dark spiral. The first lobe stops emitting and is succeeded by the radiation of the second one in Figure (c). Finally, the second light lobe also stops emitting in Figure (d), and in Figure (a) the two vortices are completely merged, whilst a new pairing process is beginning.

As shown by Mitchell's simulations,[2] vortex pairing generates sound during the rotation of the two vortices. A peak in amplitude is reached when the two vortices coalesce, and the amplitude diminishes significantly after merger. In our case, emission time associated to a vortex pair lasted for a pairing period T_p. Thus, the subsequent pairing radiations are perfectly matched. Indeed, no discontinuity can be observed between wavefronts produced by successive pairings (there is discontinuity when emission time is less than a pairing period), and the radiations of two pairings cannot interfere (there is interference when emission time is greater than a pairing period).

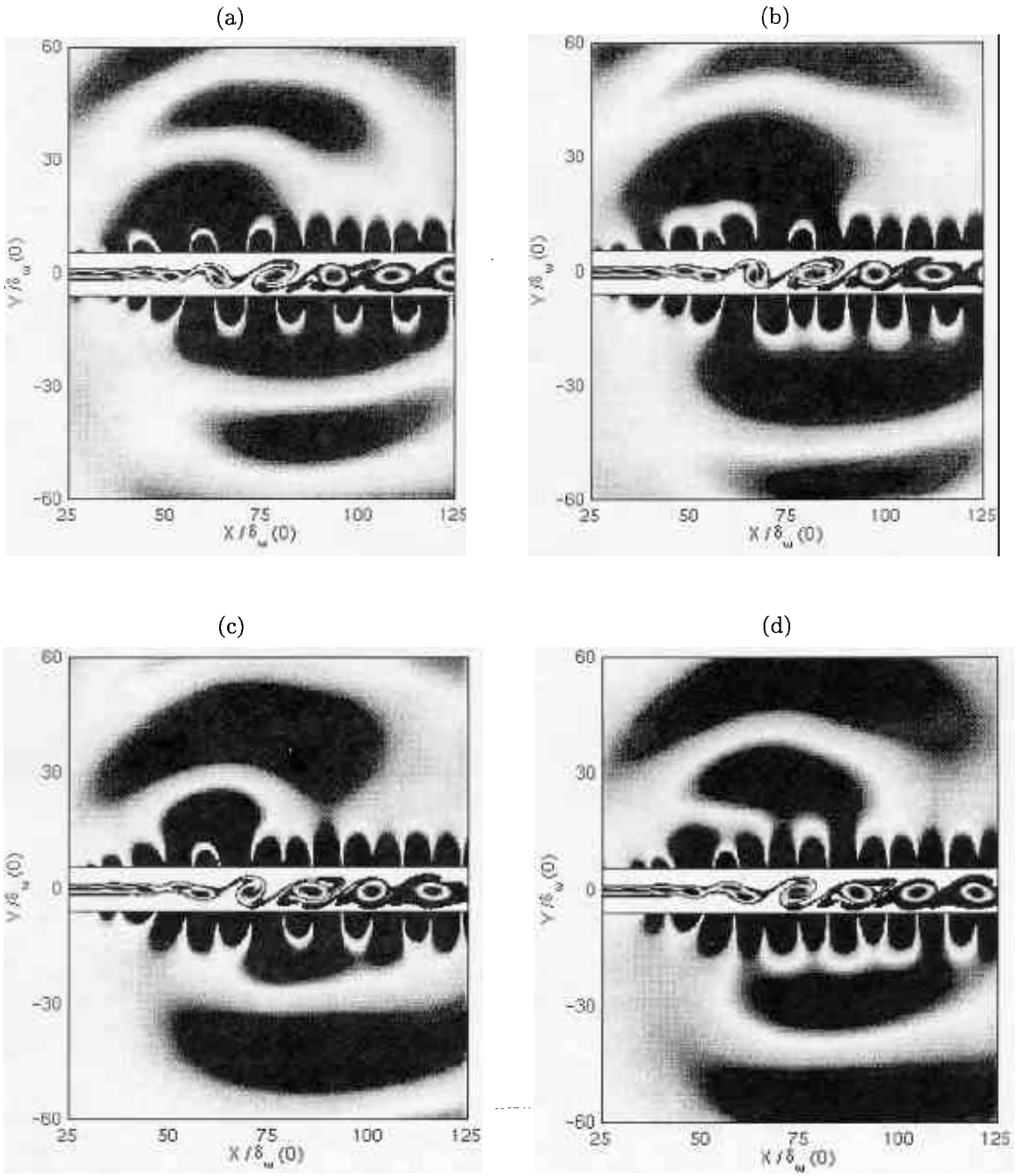

Figure 5: Four views of the vortex pairing zone: vorticity field in the mixing layer, surrounded by dilatation field. Time step is $T_p/4$ between two successive pictures. The cycle (a)-(b)-(c)-(d)-(a) describes a pairing period.

This absence of interference is also due to the fact that sources travel over a very small distance, approximatly 5 $\delta_\omega(0)$, during the pairing. The two fronts radiated by a vortex pairing appear to come from two very close locations. In figure 4, the darker and lighter fronts are not exactly concentric, the darker fronts being emitted a little upstream.

Furthermore, acoustic wavelength is directly connected to the rotation speed of the two vortices. To produce acoustic radiation with a wavelength provided by the pairing frequency f_p, the rotation speed must correspond to half this frequency, owing to the quadrupolar source. In other words, vortices complete half a revolution during the pairing period T_p. This is illustrated in the figures: from (a) to (c), a quarter revolution is observed, from (c) to (a), another quarter. Moreover, the figure (a) shows, side by side, the two orientations of the vortex pair before and after a period T_p, and in this time they complete half a revolution.

The dynamics of pairings is then at the origin of the regular wave front pattern with no interference. The acoustic wavelength is given by the pairing frequency f_p, since the co-rotative vortex pair completed half a rotation during each pairing period.

Figure 4 shows that the acoustic directivity reaches a maximum for observation angles close to 80°. This result can be attributed to the sudden merger, which increases the levels of radiation according to Mitchell simulations.[2] Refraction effects can also be invoked, even if shear thickness is very small compared to the acoustic wavelength.

5. Lighthill 's acoustic analogy

In this section, Lighthill's analogy is applied using LES aerodynamic fluctuations. Refraction and convection effects are not taken into account. Their impact on the sound field will be deduced by comparison with the direct calculation.

5.1 Theory

This theory presents the noise radiated by turbulent flows as a solution of a wave operator. Indeed, Lighthill[3] rearranges the conservation equations to give

$$\frac{\partial^2 \rho'}{\partial t^2} - c_0^2 \Delta \rho' = \frac{\partial^2 T_{ij}}{\partial x_i \partial x_j}$$

where T_{ij} is the Lighthill's stress tensor defined as

$$T_{ij} = \rho u_i u_j + (p' - \rho' c_0^2)\delta_{ij} - \tau_{ij}$$

which can be approximated in most cases by $T_{ij} \simeq \rho u_i u_j$. Outside the flow region, ρ' is reduced to the fluctuating acoustic density $\rho' = p'/c_0^2$, and T_{ij} is zero. The Lighthill equation can be interpreted as a wave equation in a medium at rest with a source term of quadrupolar nature, which is due to the double divergence.

The solution of the Lighthill equation is obtained by using the 3-D free space Green's function, $G(\mathbf{x},t) = \delta(t - x/c_0)/(4\pi c_0^2 x)$. Convolution of the Lighthill equation with the Green's function provides a retarded potential formulation. The space derivative integral formulation takes the form

$$p'(\mathbf{x},t) = \frac{1}{4\pi} \int_V \frac{1}{r} \frac{\partial^2 T_{ij}}{\partial y_i \partial y_j} \left(\mathbf{y}, t - \frac{r}{c_0}\right) d\mathbf{y} \qquad (2)$$

where $r = |\mathbf{x} - \mathbf{y}|$. It is then possible to compute the acoustic pressure field, if the aerodynamic field is known, by calculating this integral over the volume V including all acoustic sources.

Developments of the analogy have led to other expressions, described for exemple in the famous paper of Crighton.[24] In particular, a time derivative formulation can be written in the acoustic far-field

$$p'(\mathbf{x},t) = \frac{1}{4\pi c_0^2} \int_V \frac{r_i r_j}{r^3} \frac{\partial^2 T_{ij}}{\partial t^2} \left(\mathbf{y}, t - \frac{r}{c_0}\right) d\mathbf{y} \qquad (3)$$

This relationship is more often used than expression (2). Sarkar & Hussaini[25] have found that the use of space derivatives induces numerical errors of $O(1/M^2)$ with respect to formulation (3), where M is the convection Mach number of the acoustic sources. Thus, applications of expression (2) to low Mach-number flows require a high-order scheme for interpolation of retarded time.

5.2 Numerical results

The two integral formulations (2) and (3) are tested with the mixing layer simulated in section 3. Aerodynamic fluctuations given by LES are used to build the source terms. They are recorded every 10^{th} aerodynamic time step, which is equivalent to $T_0/16 = T_p/32$. Interpolation of the retarded time is performed with a fourth-order scheme.

The turbulent source volume is weighted in order to remove fluctuations on the outflow boundary, and so to avoid discontinuity in source terms. Figure 6 shows the axial weighted profile of $\partial^2 T_{ij}/\partial x_i \partial x_j$. The doubling of the period appears clearly after the pairing mechanism.

It also appears necessary to calculate and subtract the average of the source term in expression

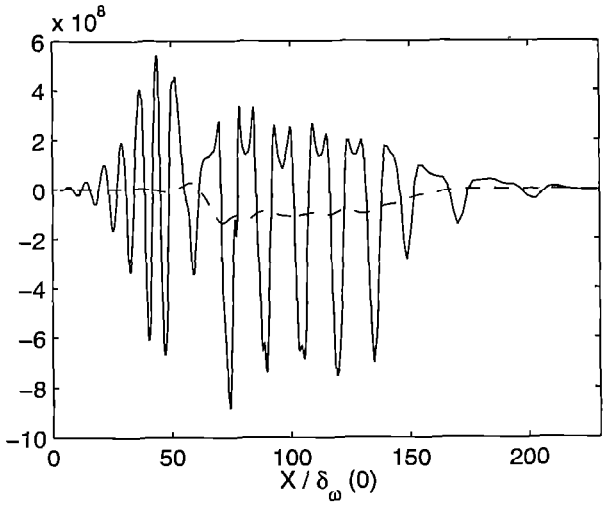

Figure 6: Axial profile of the source term. Solid line, source term $\partial^2 T_{ij}/\partial x_i \partial x_j$; dashed line, mean value of this term. Dimensional variables.

2, to obtain centered pressure fluctuations. Space source term is then given by

$$\frac{\partial^2 T_{ij}}{\partial x_i \partial x_j} - \overline{\frac{\partial^2 T_{ij}}{\partial x_i \partial x_j}}$$

The mean value cannot be neglected as illustrated in figure 6. For formulation (3), time derivatives naturally remove the mean source term.

Radiation predictions are presented in figures 7 and 8. Results of the two integral formulations are quite similar in phase and in level. However, formulation (2) is more accurate than formulation (3), as pointed out by Sarkar and Hussaini,[25] errors being greater in the upstream direction.

Formulae (2) and (3) of Lighthill's analogy ensure 3-D propagation. The levels found are then not significant. However, Lighthill's analogy provides interesting directivity patterns. They are in reasonnable agreement with the direct calculation. Two lobes of directivity close to 80° are observed, and no convection effects in the rapid flow modify sound waves. Consequently, refraction effects are very small in the direct calculation. The radiation pattern is mainly associated to noise mechanism, and not to refraction effects.

Lighthill's theory supplies reliable noise predictions, all the more accurate if the time derivative formulation (3) is used. However, it cannot be applied as a blackbox without numerical adjustments, and storage and memory requirements are significant.

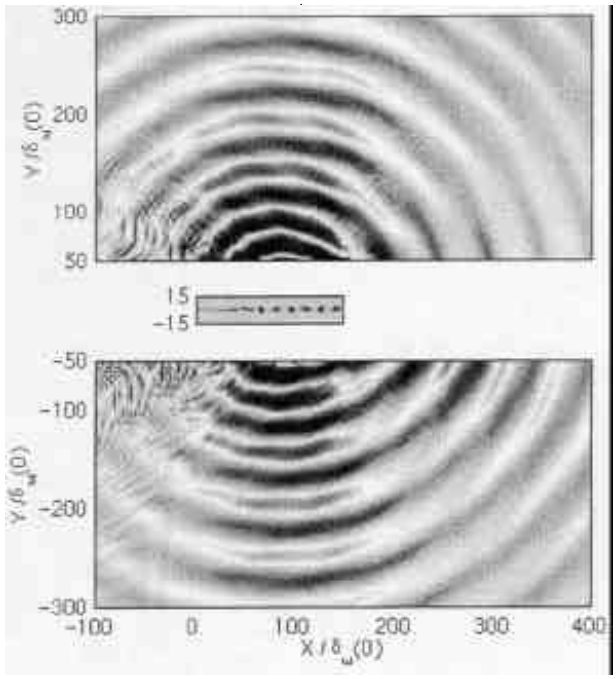

Figure 7: Pressure field calculated by the Lighthill spatial derivatives formulation.

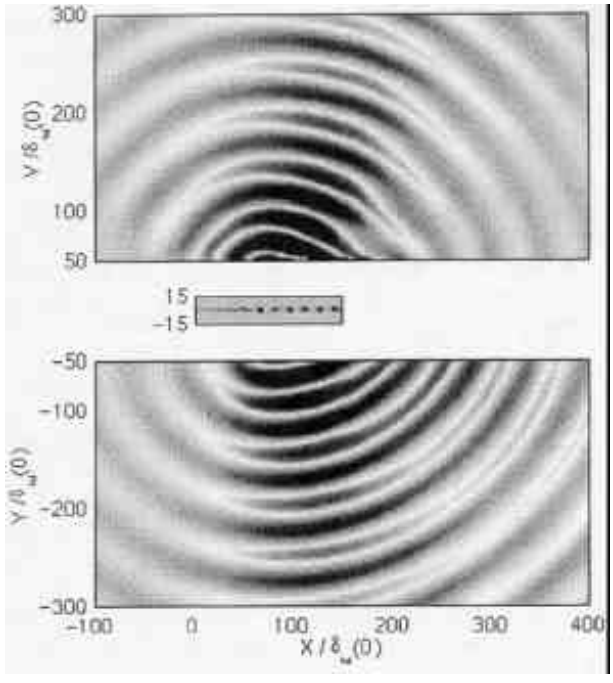

Figure 8: Pressure field calculated by the Lighthill time derivatives formulation.

6. Concluding remarks

A 2-D subsonic mixing layer was simulated to investigate its acoustic radiation. Noise was computed from Large Eddy Simulation using two approaches. In the first, the sound field is provided directly by LES, and in the second, Lighthill's analogy is applied to determine the acoustic radiation pattern from aerodynamic data. The two predictions are in good agreement. Vortex pairing constitutes an important acoustic source in subsonic low Reynolds number flow. It radiates like a rotating quadrupole, as predicted by co-rotative vortex studies. A preferred radiation direction is observed, for angles between 60° and 90°, and the noise mechanism was described in detail. Direct calculation is an attractive method in order to understand noise generation, because it supplies simultaneously turbulence and sound field data. However, full 3-D computation is required to realistically simulate turbulence and acoustic radiation, in order to allow comparisons with experimental data.

Acknowledgments

Computing time is supplied by Institut du Développement et des Ressources en Informatique Scientifique (IDRIS - CNRS). Financial support is provided by Electricité de France, Direction des Etudes et Recherches (technical monitor: P. Lafon).

References

[1]POWELL, A., 1964, Theory of vortex sound, *J. Acoust. Soc. Am.*, **36**(1), 177-195.

[2]MITCHELL, B.E., LELE, S.K. & MOIN, P., 1995, Direct computation of the sound from a compressible co-rotating vortex pair, *J. Fluid Mech.*, **285**, 181-202.

[3]LIGHTHILL, M.J., 1952, On sound generated aerodynamically - I. General theory, *Proc. Roy. Soc. London*, **211**, A 1107, 564-587.

[4]COLONIUS, T., LELE, S.K. & MOIN, P., 1997, Sound generation in a mixing layer, *J. Fluid Mech.*, **330**, 375-409.

[5]TAM, C.K.W., 1995, Computational aeroacoustics: issues and methods, *AIAA Journal*, **33**(10), 1788-1796.

[6]LELE, S.K., 1997, Computational Aeroacoustics: a review, *35th Aerospace Sciences Meeting & Exhibit*, AIAA paper 97-0018.

[7]BAILLY, C., LAFON, P., CANDEL, S., 1995, A stochastic approach to compute noise generation and radiation of free turbulent flows, 16th Aeroacoustics Conference, AIAA Paper 95-092.

[8]MITCHELL, B.E., LELE, S.K. & MOIN, P., 1997, Direct computation of Mach wave radiation in an axisymmetric supersonic jet, *AIAA Journal*, **35**(10), 1574-1580.

[9]MANKBADI, R.R., SHIH, S.H., HIXON, R. & POVINELLI, L.A., 1995, Direct computation of sound radiation by jet flow using large-scale equations, *33rd Aerospace Sciences Meeting and Exhibit*, Reno, NV, January 9-12, AIAA-95-0680.

[10]FREUND, J.B., LELE, S.K. & MOIN, P., 1998, Direct simulation of a Mach 1.92 jet and its sound field, *4th AIAA/CEAS Aeroacoustics Conference*, Toulouse, France, June 2-4, AIAA-98-2291.

[11]TAM, C.K.W. & WEBB, J.C., 1993, Dispersion-relation-preserving finite difference schemes for computational acoustics, *J. Comput. Phys.*, **107**, 262-281.

[12]HU, F.Q., HUSSAINI, M.Y. & MANTHEY, J.L., 1996, Low-dissipation and low-dispersion Runge-Kutta schemes for computational acoustics, *J. Comput. Phys.*, **124**, 177-191.

[13]TAM, C.K.W. & DONG, Z., 1995, Radiation and outflow boundary conditions for direct computation of acoustic and flow disturbances in a nonuniform mean flow, AIAA Paper 95-007.

[14]ICASE / NASA, 1995, Workshop on benchmark problems in computational aeroacoustics, NASA CP 3300, edited by Hardin, J.C., Ristorcelli, J.R. & Tam, C.K.W.

[15]BÉRENGER, J.-P., 1994, A perfectly matched layer for the absorption of electromagnetic waves, *J. Comput. Phys.*, **114**, 185-200.

[16]SMAGORINSKY, J.S., 1963, General circulation experiments with the primitive equations: I. the basic experiment, *Mon. Weath. Rev.*, **91**, 99-163.

[17]GERMANO, M., PIOMELLI, U., MOIN, P., CABOT, W.H., 1991, A dynamic subgrid-scale eddy viscosity model, *Phys, Fluids A*, **3**(7), 1760-1765.

[18]CROW, S.C. & CHAMPAGNE, F.H., 1971, Orderly structure in jet turbulence, *J. Fluid Mech.*, **48**(3), 547-591.

[19]BROWN, G.L. & ROSHKO, A., 1974, On density effects and large structure in turbulent mixing layers, *J. Fluid Mech.*, **64**(4), 775-816.

[20]WINANT, C.D. & BROWAND, F.K., 1974, Vortex pairing: the mechanism of turbulent mixing layer growth at moderate Reynolds number, *J. Fluid Mech.*, **63**(2), 237-255.

[21]MICHALKE, A., 1964, On the inviscid instability of the hyperbolic-tangent velocity profile, *J. Fluid Mech.*, **19**, 543-556.

[22]STANLEY, S. & SARKAR, S., 1997, Simulations of spatially developing two-dimensional shear layers and jets, *Theoret. Comput. Fluid Dynamics*, **9**, 121-147.

[23]HUSSAIN, A.K.M.F., 1983, Coherent structures-reality and myth, *Phys. Fluids*, **26**(10), 2816-2850.

[24]CRIGHTON, D., 1975, Basic principles of aerodynamic noise generation, *Prog. Aerospace Sci.*, **16**(1), 31-96.

[25]SARKAR, S. & HUSSAINI, Y., 1993, Computation of the acoustic radiation from bounded homogeneous flows, J. C. H. M. Y. Hussaini, in Computational aeroacoustics, *Springer-Verlag*, 335-355.